Height analysis of amorphous and crystalline ice structures on Cu(111) in scanning tunneling microscopy

2009 New J. Phys. 11 093015

(http://iopscience.iop.org/1367-2630/11/9/093015)

New Journal of Physics
The open-access journal for physics

Height analysis of amorphous and crystalline ice structures on Cu(111) in scanning tunneling microscopy

Michael Mehlhorn and Karina Morgenstern[1]
Institut für Festkörperphysik, Abteilung ATMOS, Leibniz Universität Hannover, Appelstr. 2, D-30167 Hannover, Germany
E-mail: morgenstern@fkp.uni-hannover.de

New Journal of Physics **11** (2009) 093015 (13pp)
Received 2 July 2009
Published 15 September 2009
Online at http://www.njp.org/
doi:10.1088/1367-2630/11/9/093015

Abstract. Scanning tunneling microscopy imaging of amorphous and crystalline D_2O ice on Cu(111) is discussed with respect to the apparent and the real heights of these structures above the metal surface. The apparent height increases linearly below the conduction band onset of amorphous ice and the first image state of crystalline ice, respectively. However, it largely underestimates the real height. For these voltages, histograms of the apparent height can be used to identify different layers. The dependence of the apparent height on voltage increases step-like up to the real height at the onsets of the first unoccupied electronic state. Apparent height spectroscopy is utilized to relate the apparent height to the real height of the different structures. The analysis reveals the layering during growth of porous amorphous ice between 0.1 and 1.4 BL and the dynamics of crystallization between 130 and 145 K.

[1] Author to whom any correspondence should be addressed.

Contents

1. Introduction

Scanning tunneling microscopy (STM) of molecules produces images that reflect the local electronic structure of molecules on a solid surface rather than their real-space configuration. Since the first successful images of molecules by STM [1], it has been realized that the measured height of molecules above a surface (apparent height) underestimates the real, i.e. geometric, height. Some adsorbed molecules (e.g. oxygen on several surfaces [2] or CO on Cu(111) [3]) are even imaged with a negative apparent height, i.e. as a depression in the metal surface. In addition, some molecules change contrast (oxygen/Ag(100) [4, 5], water/Ag(111) [6] and benzyne/Cu(111) [7]) from negative to positive apparent height as the bias voltage is altered. The molecules in these examples were imaged at tunneling voltages within the highest unoccupied molecular orbit (HOMO)–lowest unoccupied molecular orbit (LUMO) gap of the molecule as are many loosely bound molecules. The discrepancy between the real and the apparent height measured by STM further increases for increasing layer thickness [8]. The examples demonstrate the difficulty to determine geometric heights of molecular structures from STM images.

The real height of layered insulating structures was determined by imaging at voltages, which correspond to their conduction or valence band [9]. An equivalent method that images the molecules at a voltage corresponding to their LUMO or HOMO [10] cannot be used for molecules that are easily disturbed by the imaging procedure. Park *et al* used a combination of STM with atomic force microscopy (AFM) to investigate the height of alkylthiol molecules on Au(111) [11]. However, even heights determined by non-contact AFM should be interpreted with caution because of residual electrostatic forces as demonstrated for C_{60} on highly oriented pyrolitic graphite (HOPG) [12].

An example for a molecule that is easily disturbed by the imaging procedure is water [6], a molecule that forms extended hydrogen-bonded networks often named ‘bilayer ice’. A bilayer corresponds to one (0001) plane of bulk ice Ih [13], which consists of hexagonal rings. Three water molecules in each ring are bound via the lone-pair orbitals of the oxygen to the surface. Another three water molecules above them complete the hydrogen bonded ‘bilayer’ structure. Alternating molecules within the hexagonal rings are raised or lowered by 48 pm relative to the central plane to give the proper tetrahedral bonding angles. Hexagonal ice islands were

found on hexagonal surfaces for submonolayer coverages in islands of different dimensionalities [14, 15]. On Cu(111), we found crystalline ice islands based on the bilayer structure at around 1 BL coverage [16]. To our knowledge, the apparent height of these and other water structures has not yet been investigated systematically.

In this paper, we discuss details of STM imaging of both amorphous and crystalline ice (D_2O) structures on Cu(111) presented with a different focus in short articles before [16, 17]. Here, we first discuss the coverage dependence of the amorphous ice by analyzing apparent height histograms. We then give details about the formation of different ice structures at temperatures between 118 and 145 K. This part of the study gives insight into the kinetics of crystalline ice formation. We introduce an apparent height spectroscopy that allows the determination of the real height of the structures. The apparent height spectroscopy should be applicable to other molecular structures that are sensitive to the imaging process.

2. Experimental section

The experiments were performed with a custom-built low-temperature STM [18]. The STM facilitates measurements at 0.5 pA. This low current is important for this study because of the large difference between apparent and real height of more than 1 nm for the ice structures that demands a large surface–tip distance to avoid crashing the tip into the structures. The STM is housed in an UHV chamber with standard facilities for sample cleaning. Its base pressure is below 10^{-10} mbar.

The single crystalline Cu(111) surface is cleaned by cycles of Ne^+ sputtering and annealing. The D_2O is degassed in vacuum through freeze-thaw cycles. To minimize deposition of H_2O from the stainless steel walls of the vacuum chamber by exchange reaction, it is flushed with D_2O prior to deposition. The D_2O is brought directly to the surface held at 88 K through a molecular tube doser with a rate of 0.3 BL min^{-1}.

Measurements are performed at 5 K in constant current mode. Voltages are applied to the sample with respect to the tip. STM images are displayed in gray scale such that darker (brighter) corresponds to approach (retraction) of the tip to (from) the sample and thus smaller (larger) apparent height.

Images were taken in the course of 11 months and thus with a large variety of tips, both on the microstructure level and on a macroscopic level. From the thousands of images the ones shown here were chosen to represent a large variety of voltage and current combinations.

The STM images consist typically of 512 pixel by 512 pixel. We determine a pixel histogram with WSxM, a freeware program from Nanotec Electronica S.L.

3. Results and discussion

3.1. Ice structures on Cu(111) at different annealing temperatures

We first review the different structures that form between 88 and 145 K [16, 17]. Adsorption of approximately 1 BL of D_2O on Cu(111) at 88 K leads to a porous form of amorphous ice. This amorphous ice (figures 1(a) and (b)) is characterized by small separated clusters without long-range order.

Annealing at 118 K results into compact amorphous ice (called amorphous solid water, ASW, figure 1(c)). This form of amorphous ice differs from the ice deposited at 88 K

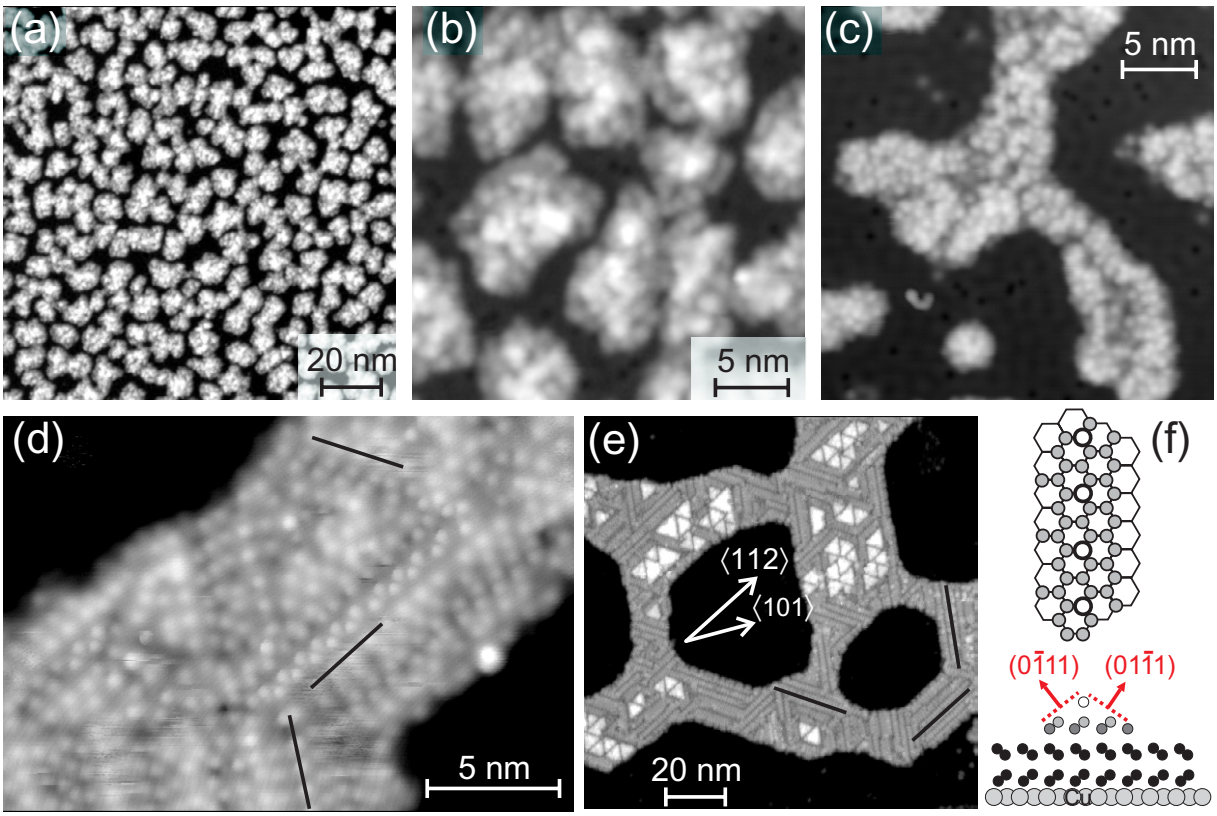

Figure 1. STM images of 1.1 BL of (a,b) porous amorphous ice as deposited at 88 K, (c) amorphous solid water obtained by flashing to 118 K, (d) ice crystallized by annealing at 130 K and (e) ice crystallized by annealing at 145 K; lines in (d,e) mark direction of ridges; surface directions are indicated in (f) and are identical in all images: (a) 1.1 pA, 140 mV; (b) 0.95 pA, 133 mV; (c) 10 pA, 55 mV; (d) 330 pA, 241 mV; (e) 1.4 pA, 1.45 V; (f) top view and side view of ridges; hexagonal grid in top view represents underlying bilayer structure; solid circles denote molecules in the third bilayer, open circles those in the fourth bilayer.

by a smaller apparent volume without desorption as verified by mass spectrometry. The change in volume is deduced from larger areas of exposed surface without an increase in apparent height (see below). Further annealing leads to crystalline ice that consists of bilayer structures terminated by facets equivalent to Ih{1110} or Ic{221}. The facets form solely ridges after annealing at 130 K (figure 1(d)) and additional truncated pyramids above 145 K (figure 1(e)) [16]. A structural model of the ridges is shown in figure 1(f). They consist of two complete bilayers with the same buckling and lattice constant as a non-supported Ih crystal, one partial bilayer, and an additional row of molecules with (2×1) arrangement, i.e. 3.5 BL in total. The partial bilayer in connection with the additional row of molecules form facets of Ih{1101} or Ic{221}. Two opposite facets form ridges that are visible as stripes in the STM image. The ridges and the sides of the pyramids are in parallel to the ⟨112⟩-direction of the Cu(111) surface. This indicates commensurate growth.

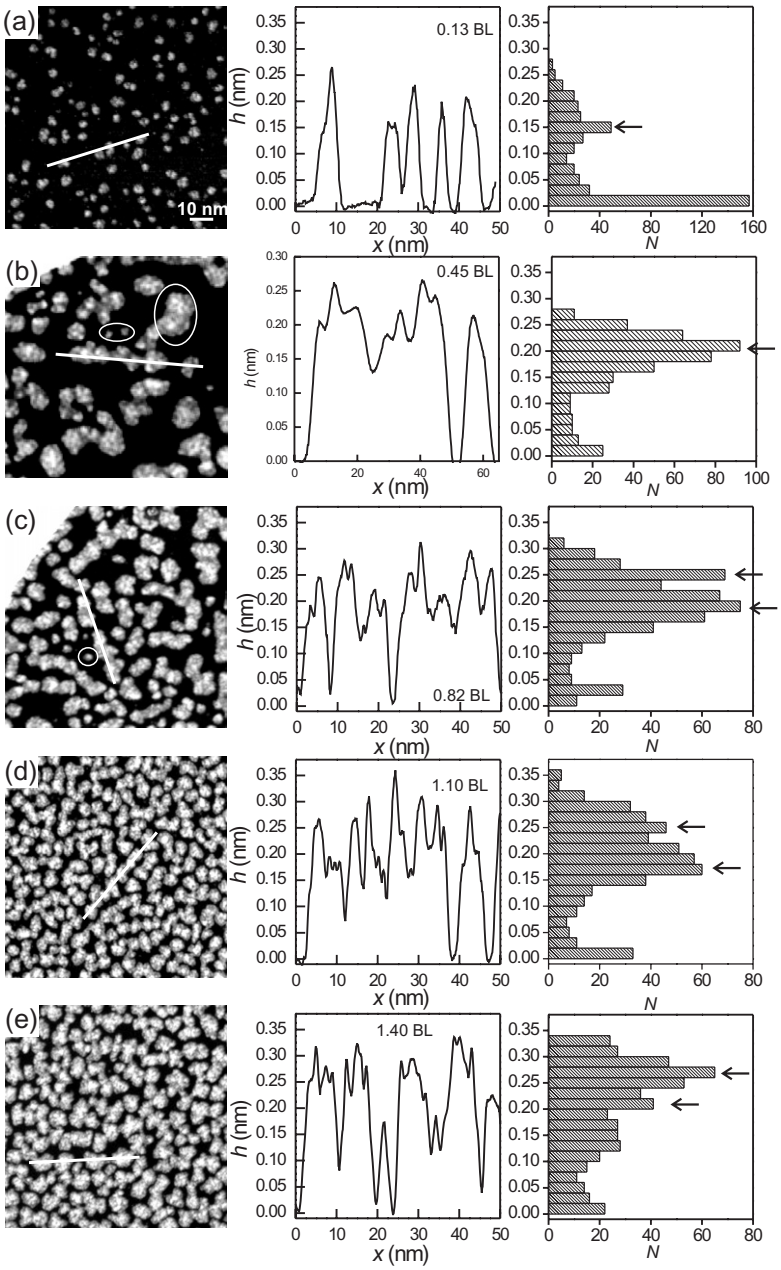

Figure 2. STM images of porous amorphous ice grown at 88 K at different coverage (left row) with line scans (middle row) as indicated in the STM images, and histograms of line scans (right row); arrows mark maxima (a) 0.13 BL, 140 mV, 8.0 pA; (b) 0.45 BL, 100 mV, 6.6 pA; (c) 0.82 BL, 310 mV, 1.0 pA; (d) 1.1 BL, 210 mV, 1.1 pA; (e) 1.4 BL, 140 mV, 1.1 pA.

3.2. Apparent height of as deposited ice

After this short review, we first analyze the apparent height of the porous amorphous ice at different coverages (figure 2). The line scans demonstrate an overall increase in average apparent height with increasing coverage (figure 2, middle row). Such a line scan is analyzed by counting

the pixels of it at a certain height and display this count in the form of histograms (figure 2, right row). At the lowest coverage of 0.13 BL (figure 2(a)) the histogram of such a line scan displays only one maximum at 0.15 nm, though the line scan itself reveals already growth in the next layers. For 0.45 BL (figure 2(b)), we observe three types of clusters. The smallest clusters are similar to the ones already observed at the lower coverage and would give rise to the same maximum in the histogram of a line scan. Two of those and one of the largest ones are encircled in figure 2(b). The largest clusters resemble those at higher coverage (see below). The majority of the clusters are in height and size in between these two types and the line scan over these (figure 2(b)) reveals a maximum at around 0.2 nm. At 0.82 BL, the smallest type of the clusters is rare and the two larger types coexist. A line scan crossing these (figure 2(c)) leads to a histogram with two maxima at 0.2 and 0.25 nm. The smallest type of islands is no longer observable at 1.1 or 1.4 BL. The histograms of the line scans show the same maxima as before. In summary, line scans of the porous amorphous ice structures show maxima at approx. 0.15, 0.2 and 0.25 nm. The existence of the maxima suggests that the molecules have some surface-induced vertical order up to three distinct layers. Similar ordering was observed for fluid water close to a surface [19]–[21].

The first maximum is with 0.15 nm considerably lower than the distance of a single molecule above the surface [22]. The next two layers have an apparent height of 0.05 nm each. It is expected that additional insulating 'layers' have decreasing apparent height. However, this is not observed for the third layer. The decrease might be undetectable within the error bar. Alternatively, it might indicate that the layer thickness increases with increasing distance from the surface. This is again in analogy to fluid water [19]–[21]. Note that the maxima shift slightly to higher values at higher voltage and that the maxima vary in position for the different histograms.

3.3. Apparent height of annealed ice

We now investigate the apparent height of the annealed structures (figures 1(c)–(e)) by analyzing STM images that show molecular resolution in the top layer (e.g. figures 3(a) and (b)). In this investigation, we concentrate on a fixed coverage of 1.1 BL, because a variation in coverage is found to change the lateral dimension of the structures but not their structure. The analysis reveals details on the mass transport during annealing.

The white circular protrusions show no order (figure 3(a)) indicative of amorphous ice. Their diameter of 0.6–0.7 nm identifies them as single molecules [15, 23]. Those protrusions that are not circular or show a larger diameter are several molecules that are too close to each other to be imaged as separate molecules.

The pixel histogram of the ASW ice shows two maxima at 0.16 and 0.24 nm with respect to the surface maximum at 0 nm (figure 3(c)). The values are the same as for the porous amorphous water. We thus attribute the maxima to molecules that are in the first and second bilayer above the surface. In contrast to porous amorphous water at the same coverage (cf figure 2(d)), there are almost no molecules observed in the third layer (at ≈ 0.3 nm). As no material has been desorbed and the water uncovered surface area has increased (see above) the amorphous ice adsorbed at 88 K must have been porous. The existence of such a porous form of amorphous ice was proven by N_2 adsorption–desorption experiments for ice grown on Pt(111) [24]. It was explained by a hit-and-stick deposition. In figure 2, however, the number of identifiable layers does not increase between 0.45 and 1.4 BL. This points to a certain lateral transport already

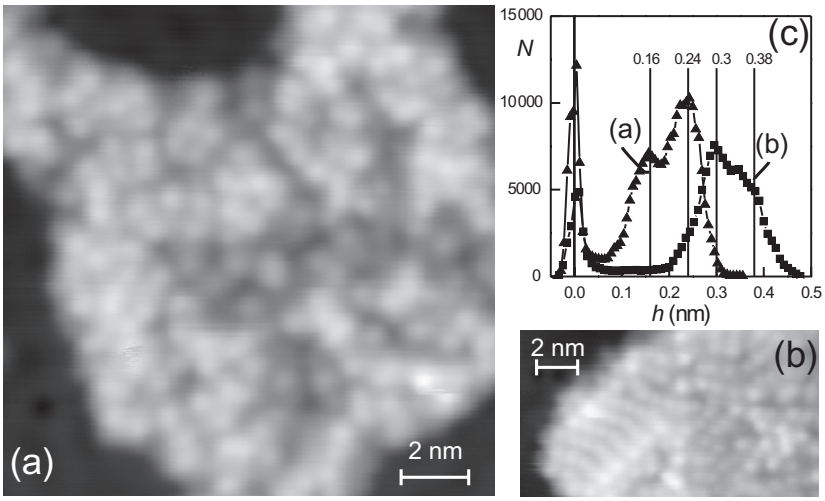

Figure 3. Comparison of ASW ice (a) and just crystallized ice (b): (a) adsorbed at 88 K and flashed to 118 K, 56 mV, 10 pA; (b) adsorbed at 88K and flashed to 130 K, 125 mV, 3 pA. (c) Height histogram of pixels in STM images; triangles from (a), squares from (b); vertical lines mark maxima of a multiple Gaussian fit.

at 88 K. Such a transport is consistent with the observed gradual decrease of porosity with temperature in [24]. A possible explanation is that more than one hydrogen bond has to be formed, before the molecule 'sticks'. Amorphous solid water was also found to grow layer-by-layer at least the first three layers on Pt(111) [25]. In difference to the ice on Cu(111), the ice wets Pt(111) facilitating to determine this layering by temperature programmed desorption experiments. The experiment on Cu(111) here thus demonstrates that layering does not require a wetting layer.

We observe here that the collapse of the pores is accompanied by a coarsening of the islands and thus that the ice does not only rearrange within the clusters but also diffuses over the surface. The form of the clusters (figure 1(c)) indicates a dominance of Smolouchowski coarsening.

We next flash the sample to 130 K. After this flash some part of the top structure shows long-range order (figure 3(b), left-hand side). In the height histogram (figure 3(c)), the lowest value of 0.16 ML disappears. Two higher values develop at 0.3 and 0.38 nm (figure 3(c)). We infer that the structure is up to four bilayers high and the two lowest ones have the same lateral size. Most of this double bilayer is covered by the facet such that the remaining peak at 0.24 nm is rather small. Separate histograms of image sections allow us to attribute the peak at 0.3 nm to the facetted part of the cluster on the left-hand side of the image and the one at 0.38 nm to the not yet ordered part of the cluster at the right-hand side of the image. We conclude that (a) molecules are transported into higher layers during crystallization and (b) first a double bilayer is formed at the water–metal interface and only subsequently the top layer orders.

After complete faceting of the top layer (figure 4(a)) the peak attributed to the unordered top structure disappears. The peak at 0.27 nm shows clear deviations from the single Gaussian. In the higher resolution histogram of the top layer only, two shoulders to the left and the right of the main peak at 0.23 and 0.3 nm, respectively, are discernible.

The layering is less obvious in the height histograms of figures 4(b) and (c) for facetted structures, because molecules from partially filled bilayers contribute to the image. This is

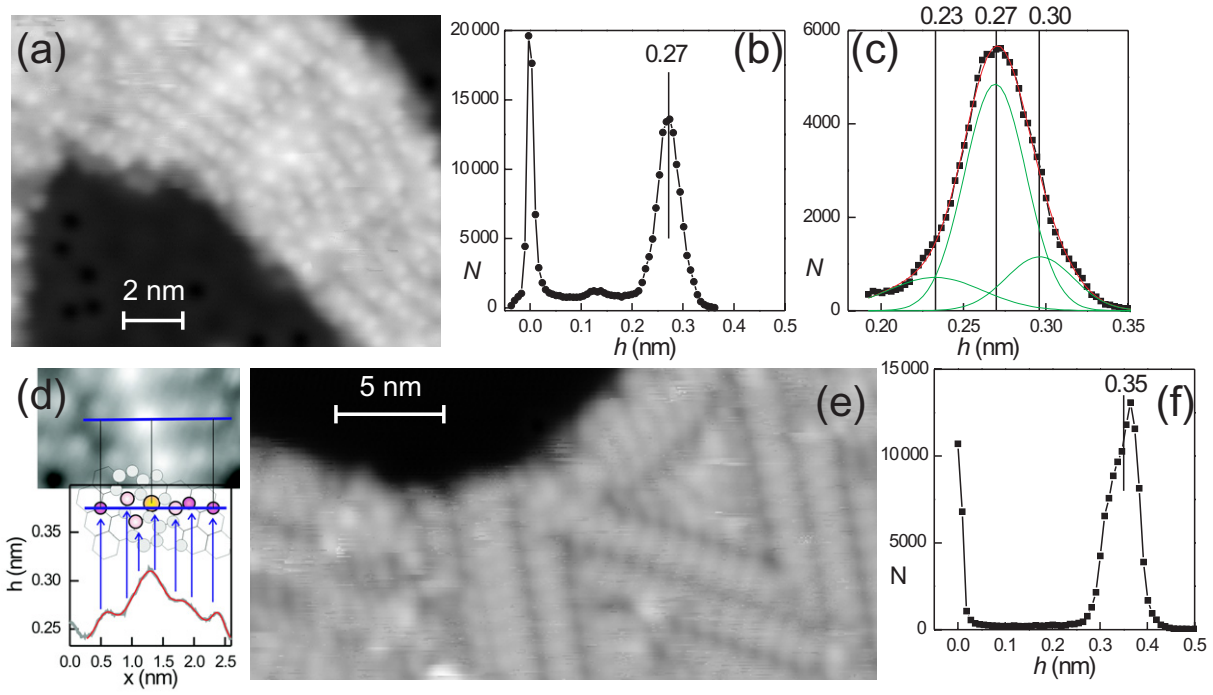

Figure 4. Completely crystallized ridges structure, adsorbed at 88 K and annealed at 130 K: (a) STM image, 4.4 pA, 114 mV; (b) height histogram of total image (a); (c) height histogram of partial image on ice island (d) line scan across facet as indicated in STM image, 0.18 V, 2.5 pA, and compared to molecule position in model of facet; position of the arrows result from fitting Gaussians to the line scan (e) STM image, 8.7 pA, 1.02 V (f) height histogram of (e).

demonstrated in the line scan shown in figure 4(d). Based on the model of the ridges shown in the inset we infer that seven molecules at three different heights influence this specific height profile. Similar line scans are observed in other directions and demonstrate the origin of the broad peak in figure 4(c).

Again, the apparent heights in the histograms are obviously too small to represent geometric heights.

As noted above for the amorphous ice, the exact positions of the maxima in the histograms are voltage dependent. At approximately five times the voltage (figures 4(e) and (f)) the main peak is again clearly a multiple peak, which is centered at 0.35 nm.

We finally report that further annealing leads to further maxima in the curves because of the formation of pyramids (figure 5). The maxima for the pyramids are at 0.49 and 0.63 nm. The 0.33 nm peak results from the ridges structure.

Pyramids of three different base lengths exist (figure 5(c)). The height thereby increases with increasing base length. The 3D view in figure 5(d) shows best that the pyramids are all truncated. The image used for the pixel histogram in figure 5(b) shows one pyramid of type 3, four pyramids of type 2 and one pyramid that just converts from type 1 to type 2. The two additional peaks at 0.5 and 0.63 nm are thus attributed to two and three additional bilayers above the double bilayer. 64% of more than 300 pyramids have a base length of (4.3 ± 0.3) nm, corresponding to ten ice unit cells. 21% of the pyramids have a base length of (2.7 ± 0.2) nm,

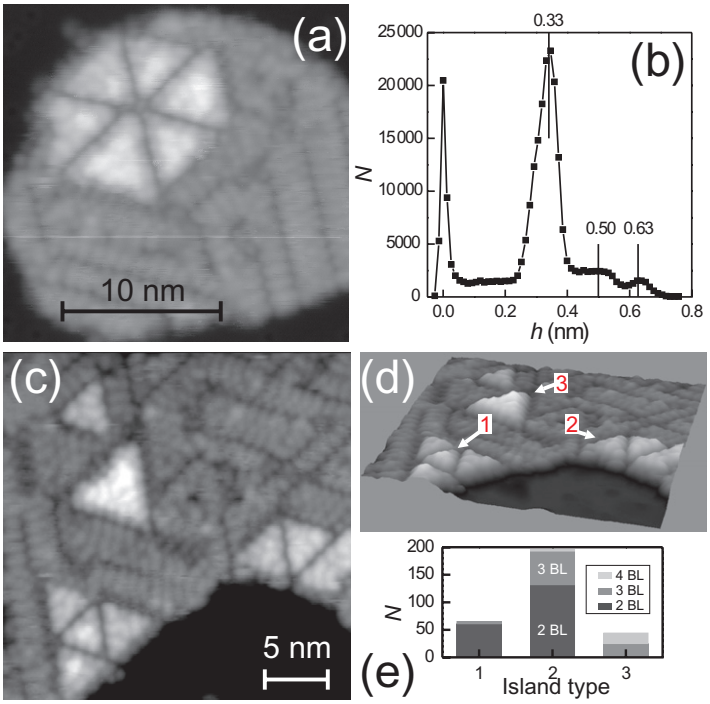

Figure 5. Pyramidal structure on top of ridges, adsorbed at 88 K and annealed at 145 K: (a) STM image 1.9 pA and 1.02 V; (b) height histogram of (a); (c) STM image, 1.4 pA, 1.73 V; (d) 3D image of (c) indicating the three most common types of pyramids; (e) distribution of islands of different types; gray shades represent average heights above the complete double bilayer.

i.e. six ice unit cells, and 15% of (6.0 ± 0.2) nm, i.e. 14 unit cells. We propose that the distinct base lengths are a result of proton ordering [26]. Figure 5(e) shows the size distribution of the pyramidal islands and the number of bilayers for the pyramids of a certain base length.

The discussion of the apparent heights of the different structures demonstrates that we may follow qualitatively the development of the structure's height by analysis of the image histograms provided we use a similar bias voltage. Thereby, we attribute each additional maximum to an additional (bi-)layer. However, the apparent height depends on voltage and the question remains to which real heights the thus determined layers correspond.

3.4. Apparent height spectroscopy

In principle, it should be possible to measure the real height by imaging the ice at voltages beyond the onset of either the conduction band [17] or the valence band [27]. However, acquiring complete STM images above the conduction band onset is obstructed here, because the electron sensitivity of the structures leads to damage, in particular at high voltage [23, 28]. We thus employ a different strategy. Fast scanning allows to take several lines of an image before the first destruction event. From those partial images, we determine the average apparent height of the ice islands.

The destruction event (desorption, hydrogen bond rearrangement, or dissociation, see [23, 28, 29]) usually leads to a considerable change in ice structure. Thus, each data point is

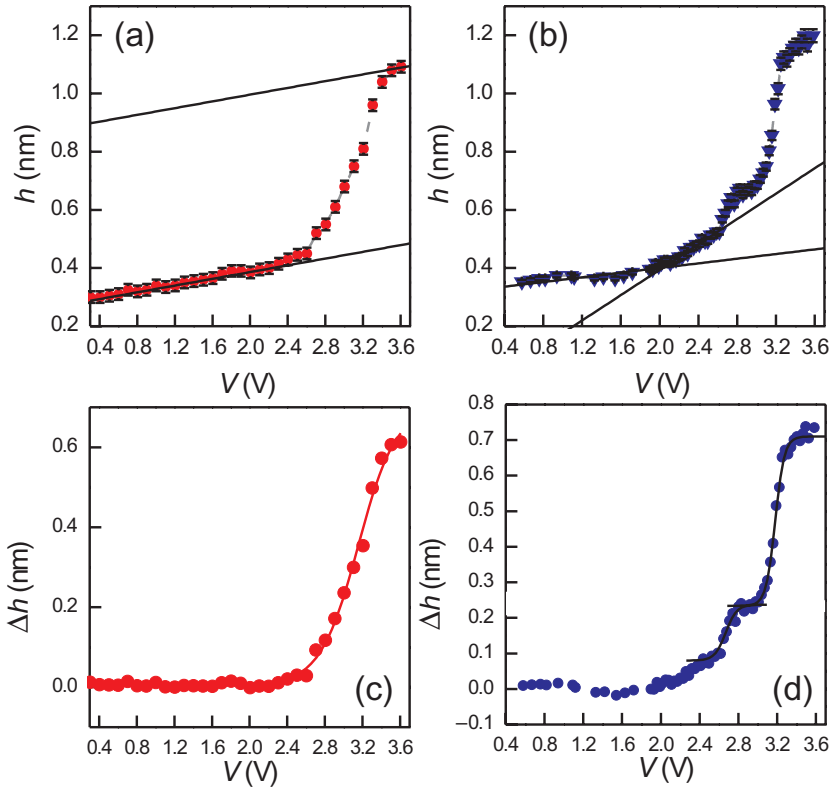

Figure 6. Average apparent height as a function of tunneling voltage for islands of amorphous ice at 1.8 pA (a, adapted from [17]) and of crystalline ice; $I = 0.5$ pA, 1.1 BL (b), (c,d) are (a,b) after subtraction of the first linear increase shown as solid lines in (a,b); (c) is fitted by one Boltzmann function rising at 3.15 ± 0.02 V with a width of 0.2 V; (d) is fitted by two increases at 2.67 and 3.18 V, with a smaller width of approx. 0.05 V.

taken at a different spot of the surface. At this pristine spot of the surface, first an image is taken at non-destructive tunneling parameters to ensure that the structures are indeed unperturbed. Then this spot is imaged at the voltage of interest.

The average apparent height is displayed against voltage in figure 6 for one of the amorphous and one of the crystalline structures. For the amorphous structure, we investigate the porous amorphous ice (figure 6(a)) and the ridges without pyramids for the crystalline structure (figure 6(b)). Note that the value displayed in figure 6 is comparable to the mean of the Gaussian peak in a histogram (e.g. in figure 4(c)).

There are several similarities in the apparent height versus voltage curves of amorphous and of crystalline ice. Both show a quasi-linear increase up to 2 V, a region of strongly enhanced increase up to 3.3 V, and again a less strong increase above 3.3 V. In the nonlinear region, the spectra differ.

In the case of amorphous ice, the apparent height is linear up to 2.4 V with a slope of $0.058\,\mathrm{nm\,V^{-1}}$ (figure 6(a)). The deviation from this constant slope can be well fitted by a Boltzmann curve at (3.15 ± 0.02) V with a width of 0.2 V (figure 6(c)).

For the crystalline ice, the increase is more complex (figure 6(b)). The increase is linear only up to approximately 2 V with a smaller slope of $0.04\,\mathrm{nm\,V^{-1}}$. There is another region of

linear increase up to approx. 2.8 V, with a much higher slope of 2.2 nm V^{-1}. Two Boltzmann-like increases are situated at 2.67 and 3.18 V (figure 6(d)).

The apparent height of a water bilayer on Pt(111) was found to change by ≈ 0.02 to 0.035 nm V^{-1} at 0.2 nA in the gap region up to ± 2 V [30]. The change is thus in the same order of magnitude as found here, though the current is lower, the coverage higher, and we investigate a different surface. Though the number of data points in the earlier work does not allow to identify a linear dependence, the comparison suggests that the linear increase might not be restricted to the specific system on Cu(111).

The strong increases observed here on Cu(111) at higher voltage can be partly understood by the electronic band structure as measured in two-photon photoemission [31, 32]. Crystalline ice exhibits the first image potential state at 3.1 eV. Amorphous ice exhibits an energetically broad conduction band with an onset at 3 V with many defect states within the gap because of the disordered structure. Both are delocalized states and are involved in the transfer of electrons from the metal to the ice layer in femtosecond laser excitation experiments. Therefore, the increase at 3.15 eV for the amorphous ice is attributed to its conduction band onset; defect states are not observed for this form of ice in apparent height spectroscopy. The second increase at approx. 3.2 V above the crystalline ice is consistent with its first image potential state.

Static local variations in the molecular environment are known to lead to localized electronic states below the conduction band [33]. The first increase in the apparent height spectrum above the crystalline ice at 2.7 V is thus attributed to defect states that result from the facets. The defects arise, because molecules have one to four hydrogen bonds within the facets. The different slope of the linear increase beyond 2 V could be related to an additional tunneling channel in STM and is thus not intrinsic to the ice structure.

We finally relate the heights measured beyond the strong increase to the layering revealed in the height histograms of images taken in the gap. For amorphous ice, the three fluid-like layers identified in figure 2 corresponds to 1.1 nm giving a reasonable average distance of 0.37 nm between the layers. For crystalline bilayers, the distance between two layers is 0.368 nm and the distance of the first bilayer above the surface is 0.31 nm [22]. We thus expect geometric heights of 0.68 nm for the double bilayer, 1.05 nm for the third, and 1.41 nm for a complete fourth bilayer. The ridges with an average geometric height of (1.18 ± 0.02) nm thus correspond to 3.5 bilayers. This is in perfect agreement with the ridges model. The same kind of analysis reveals a height of 1.5 nm for the pyramids.

We also tried to follow the same strategy in the negative voltage range, where the same effect should be observable at the onset of the valence band, expected beyond the ice gap below -5 eV. However, our tip was not stable enough to support such a high voltage. In contrast, Thürmer and Bartelt were able to image up to 30 BL of ice on Pt(111) by imaging at -6 V, the voltage of the first occupied states of ice in contact with platinum [27].

4. Conclusion

We investigated the ice structures that form on Cu(111) between 88 K and the desorption temperature. For the porous amorphous form of ice, we follow the growth between 0.1 and 1.4 BL. This amorphous ice shows a layering. Thereby, the number of layers is three inbetween 0.45 and 1.4 BL indicative of lateral molecule transport at 88 K. At 118 K, the collapse of the pores to amorphous solid water is accompanied by coarsening of the islands, indicative of the motion of ice clusters over the surface. During crystallization at 130 K an upward transport

of the molecules into higher layers is observed. Restricted to 1.2 nm above the surface for the ridges, this upward transport is increased during annealing at 145 K to 1.5 nm.

The real heights and corresponding number of bilayers above the surface were determined by apparent height spectroscopy. The latter was introduced here and rules out a possibility to determine the real height even when imaging the molecule within the HOMO–LUMO gap for both crystalline and amorphous ice structures. Above the first electronic state, the height values are very close to real heights, while the apparent height of the structures is only about one-third of their real height, when imaged within the gap. The apparent height spectroscopy should not be restricted to the system investigated here, but applicable to other molecular islands and clusters adsorbed on metal surfaces that are sensitive to electron damage provided that the density of states of metal and the overlayer are similar as in the case of water on copper [34, 35].

Acknowledgment

We acknowledge financial support from the Deutsche Forschungsgemeinschaft.

References

[1] Ohtani H, Wilson R J, Chiang S and Mate C M 1988 *Phys. Rev. Lett.* **60** 2398
Spong J K, Mizes H A, LaComb L J Jr, Dovek M M, Frommer J E and Foster J S 1989 *Nature* **338** 137
Lippel P H, Wilson R J, Miller M D, Wöll Ch and Chiang S 1989 *Phys. Rev. Lett.* **62** 171
[2] Wintterlin J, Brune H and Behm R J 1988 *Appl. Phys.* A **47** 99
[3] Meyer G, Neu B and Rieder K H 1995 *Chem. Phys. Lett.* **240** 379
[4] Schintke S, Messerli S, Morgenstern K, Nieminen J and Schneider W-D 2001 *J. Chem. Phys.* **114** 4206
[5] Nieminen J, Lahti S, Paavilainen S and Morgenstern K 2002 *Phys. Rev.* B **66** 165421
[6] Morgenstern K and Nieminen J 2004 *J. Chem. Phys.* **120** 10786
[7] Simic-Milosevic V, Bocquet M-L and Morgenstern K 2009 *Surf. Sci.* **603** 2479
[8] Hebenstreit W, Redinger J, Horozora Z, Schmid M, Podlocky R and Varga P 1999 *Surf. Sci.* **424** L321
[9] Gallagher M C, Fyfield M S, Bumm L A, Cowin J P and Joyce S A 2003 *Thin Solid Films* **445** 90
Olsson F E, Persson M, Repp J and Meyer G 2005 *Phys. Rev.* B **71** 075419
[10] Parisse P, Passacantando M and Ottaviano L 2006 *Appl. Surf. Sci.* **252** 7469
[11] Park J Y, Qi Y, Ratera I and Salmeron M 2008 *J. Chem. Phys.* **128** 234701
[12] Sadewasser S and Lux-Steiner M Ch 2003 *Phys. Rev. Lett.* **91** 266101
[13] Henderson M A 2002 *Surf. Sci. Rep.* **46** 5
[14] Cerda J, Michaelides A, Bocquet M-L, Feibelman P J, Mitsui T, Rose M, Fomin E and Salmeron M 2004 *Phys. Rev. Lett.* **93** 116101
Yamada T, Tamamori S, Okuyama H and Aruga T 2006 *Phys. Rev. Lett.* **96** 036105
[15] Michaelides A and Morgenstern K 2007 *Nat. Mater.* **6** 597
[16] Mehlhorn M and Morgenstern K 2007 *Phys. Rev. Lett.* **99** 246101
[17] Stähler J, Mehlhorn M, Bovensiepen U, Meyer M, Kusmierek D O, Morgenstern K and Wolf M 2007 *Phys. Rev. Lett.* **98** 206105
[18] Mehlhorn M, Gawronski H, Nedelmann L, Grujic A and Morgenstern K 2007 *Rev. Sci. Instrum.* **78** 033905
[19] Schweighofer K J, Xia X and Berkowitz M L 1996 *Langmuir* **12** 3747
[20] Price D L 2000 *J. Chem. Phys.* **112** 2973
[21] Izvekov S and Voth G A 2001 *J. Chem. Phys.* **115** 7196
[22] Michaelides A 2008 private communication
[23] Morgenstern K and Rieder K-H 2002 *Chem. Phys. Lett.* **358** 250
[24] Stevenson K P, Kimmel G A, Dohnalek Z, Smith R S and Kay B D 1999 *Science* **283** 1505

[25] Kimmel G A, Petrik N G, Dohnalek Z and Kay B D 2006 *J. Chem. Phys.* **125** 044713
[26] Pan D, Liu L-M, Tribello G A, Slater B, Michaelides A and Wang E 2008 *Phys. Rev. Lett.* **101** 155703
[27] Thürmer K and Bartelt N C 2008 *Phys. Rev.* B **77** 195425
Thürmer K and Bartelt N C 2008 *Phys. Rev. Lett.* **100** 186101
[28] Mehlhorn M, Gawronski H and Morgenstern K 2008 *Phys. Rev. Lett.* **101** 196101
[29] Morgenstern K and Rieder K-H 2002 *J. Chem. Phys.* **116** 5746
Morgenstern K, Gawronski H, Mehlhorn M and Rieder K-H 2004 *J. Mod. Opt.* **51** 2813
Gawronski H, Morgenstern K and Rieder K-H 2005 *Eur. Phys. J.* D **35** 349
Gawronski H, Carrasco J, Michaelides A and Morgenstern K 2008 *Phys. Rev. Lett.* **101** 136102
[30] Morgenstern M, Müller J, Michely Th and Comsa G 1997 *Z. Phys. Chem.* **198** 43
[31] Gahl C, Bovensiepen U, Frischkorn Ch and Wolf M 2002 *Phys. Rev. Lett.* **89** 107402
[32] Bovensiepen U, Gahl C and Wolf M 2003 *J. Phys. Phys.* B **107** 8706
[33] Zallen C R 1983 *The Physics of Amorphous Solids* (New York: Wiley)
[34] Snow E C 1968 *Phys. Rev.* **171** 785
[35] Petrenko V F and Ryzhkin I A 1993 *Phys. Rev. Lett.* **71** 2626